NANO LETTERS

Letter

pubs.acs.org/NanoLett

Ambient-Air Stable Lithiated Anode for Rechargeable Li-Ion Batteries with High Energy Density

Zeyuan Cao,[†] Pengyu Xu,[†] Haowei Zhai,[†] Sicen Du,[†] Jyotirmoy Mandal,[†] Martin Dontigny,[‡] Karim Zaghib,[‡] and Yuan Yang*[,†]

[†]Program of Materials Science and Engineering, Department of Applied Physics and Applied Mathematics, Columbia University, New York 10027, New York

[‡]IREQ—Institute Recherche d'Hydro-Québec, 1800 Boulevard Lionel Boulet, Varennes, Quebec J3X 1S1, Canada

Supporting Information

ABSTRACT: An important requirement of battery anodes is the processing step involving the formation of the solid electrolyte interphase (SEI) in the initial cycle, which consumes a significant portion of active lithium ions. This step is more critical in nanostructured anodes with high specific capacity, such as Si and Sn, due to their high surface area and large volume change. Prelithiation presents a viable approach to address such loss. However, the stability of prelithiation reagents is a big issue due to their low potential and high chemical reactivity toward O_2 and moisture. Very limited amount of prelithiation agents survive in ambient air. In this research, we describe the development of a trilayer structure of active material/polymer/lithium anode, which is stable in ambient air (10−30% relative humidity) for a period that is sufficient to manufacture anode materials. The polymer layer protects lithium against O_2 and moisture, and it is stable in coating active materials. The polymer layer is gradually dissolved in the battery electrolyte, and active materials contact with lithium to form lithiated anode. This trilayer-structure not only renders electrodes stable in ambient air but also leads to uniform lithiation. Moreover, the degree of prelithiation could vary from compensating SEI to fully lithiated anode. With this strategy, we have achieved high initial Coulombic efficiency of 99.7% in graphite anodes, and over 100% in silicon nanoparticles anodes. The cycling performance of lithiated anodes is comparable or better than those not lithiated. We also demonstrate a $Li_4Ti_5O_{12}$/lithiated graphite cell with stable cycling performance. The trilayer structure represents a new prelithiation method to enhance performance of Li-ion batteries.

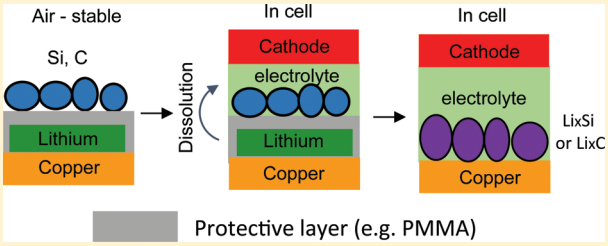

KEYWORDS: *prelithiation, silicon anode, PMMA, energy storage, Coulombic efficiency, solid electrolyte interphase*

Rechargeable Li-ion batteries (LIBs) with high energy density are attractive for applications ranging from portable electronics to electric vehicle and grid-level energy storage.[1,2] State-of-the-art LIBs are produced in the discharged state because the electrode materials are air-stable.[3,4] However, a considerable amount of active Li^+ ions is lost in the initial charge due to the formation of the solid electrolyte interphase (SEI) on the anode surface, which results in a low initial Coulombic efficiency and lowers the energy density of full cells.[5,6] This loss is 5−20% of total available capacity in commercial graphite electrodes, and it could reach 15−50% for next-generation anode materials with high capacity (e.g., Si and Sn),[6−11] because these materials have large volume expansion and high surface area, especially when nanostructured electrodes are used to improve cycling performance and power capability.[8−12] The high initial loss of Li reduces achievable capacity in a full cell and thus compromises the gain in energy density and cycling life of these nanostructured electrodes. Accordingly, there is a strong motivation to prelithiate the anode to compensate the Li loss during SEI formation.

Various methods have been developed to prepare lithiated anode, such as electrochemical/chemical lithiation,[13−15] lithium-rich electrode additives,[16−18] and protected lithium particles.[19,20] However, many lithium-rich additives[15,16] and protected lithium particles[19,20] are not stable in ambient air with relative humidity (RH) well beyond that in dry rooms. Therefore, they are mainly used in the dry room (RH < 1%), which increases fabrication cost. Moreover, the addition of lithiated particles could lead to inhomogeneity in active electrode materials and current distribution, and consequently promote dendrite formation.[21] To address these issues, we propose a strategy to prepare an ambient-air-stable lithiated anode with uniform distribution of lithium source. The electrode is stable in air with RH of 10−30% for over 60 min, which could allow manufacturing at large scale. Moreover, the polymeric protective layer in our design is readily soluble in the electrolyte, and thus no excessive inactive materials, such as protective Li_2O or Li_2CO_3 layer,[16,19] stay in the battery and reduce battery energy density. In addition, the amount of

Received: August 30, 2016
Revised: September 26, 2016
Published: October 3, 2016

DOI: 10.1021/acs.nanolett.6b03655
Nano Lett. 2016, 16, 7235−7240

lithium in the anode is easily tuned from simply compensating SEI to fully lithiating all anode materials by controlling the thickness of the lithium layer. The latter case allows the lithiated anode to pair with high capacity Li-free cathode materials (e.g., S, O_2) to further improve the energy density of LIBs.[13,22]

The proposed strategy is illustrated in Figure 1. First, lithium deposited on a Cu foil is coated with a protective polymer layer

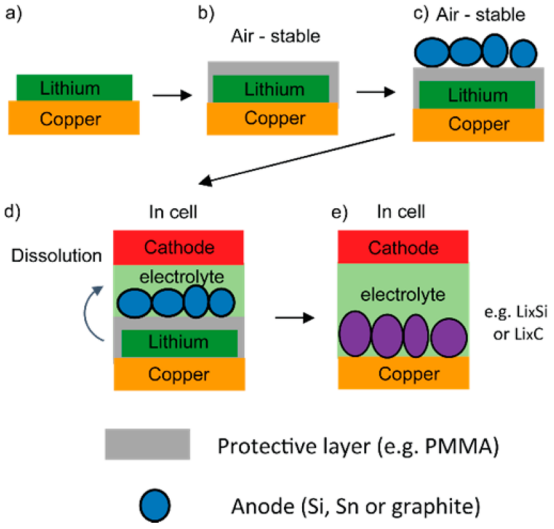

Figure 1. Schematic of the process to prepare ambient-air-stable lithiated anode: (a) Li is deposited on Cu film, (b) polymer (e.g., PMMA) is coated on Li surface to make it air-stable, (c) anode materials are coated onto Li with a solvent that does not dissolve PMMA (e.g., ethanol or water), (d) the anode and the cathode are assembled together with organic electrolyte injected, which dissolves polymer coating, and (e) anode materials are lithiated as they contact with Li due to pressure inside the cell.

to render it ambient-air-stable. Then, the anode materials (e.g., graphite or Si) are deposited onto the polymer with a solvent that does not dissolve it. As the metallic lithium and anode materials are separated by the polymer layer, this trilayer anode is stable even in ambient air. The anode is integrated with conventional cathode materials, then a battery electrolyte is added to form a battery. The polymer coating layer (e.g., poly(methyl methacrylate), PMMA) is carefully selected to be soluble in the battery electrolyte (e.g., carbonate-based). Therefore, the anode materials in the cell contact lithium as a result of pressure inside the cell, and forms a lithiated anode. In such a process, neither the metallic lithium nor the lithiated anode are exposed to air, and thus, they survive in the ambient air environment. Furthermore, the lithiation is uniform because the lithium film distributes evenly on the copper substrate. The critical point is to find a polymer that is insoluble in the anode slurry solution but soluble in commercial carbonate-based battery electrolytes. In this report, PMMA is selected as a model example. It is readily soluble in carbonate-based electrolytes with a solubility over 20 wt %, but insoluble in ethanol and water, which are widely studied and even used in commercial processes for coating anode materials.[23−25] Moreover, PMMA is widely used in a gel electrolyte, which is compatible with the electrochemical environment in Li-ion batteries.[26−28] Impedance measurements also show that even with 20% PMMA, the battery electrolyte still has an ionic conductivity of 1.7 mS/cm at room temperature, which is reasonable for Li-ion batteries. In this report, graphite and silicon in ethanol with poly(acrylic acid) (PAA) binder are used as the coating slurry, and the compatibility of PMMA-coated lithium with water is also discussed.

To prepare the graphite/PMMA/Li trilayer structure, lithium was first electrochemically deposited on copper from 1 M lithium bis(trifluoromethane)sulfonimide (LiTFSI) in 1,3-dioxolane (DOL) with 1 wt % $LiNO_3$, which shows a fiber-like structure (Figure 2a). The cross section view (Figure 2b)

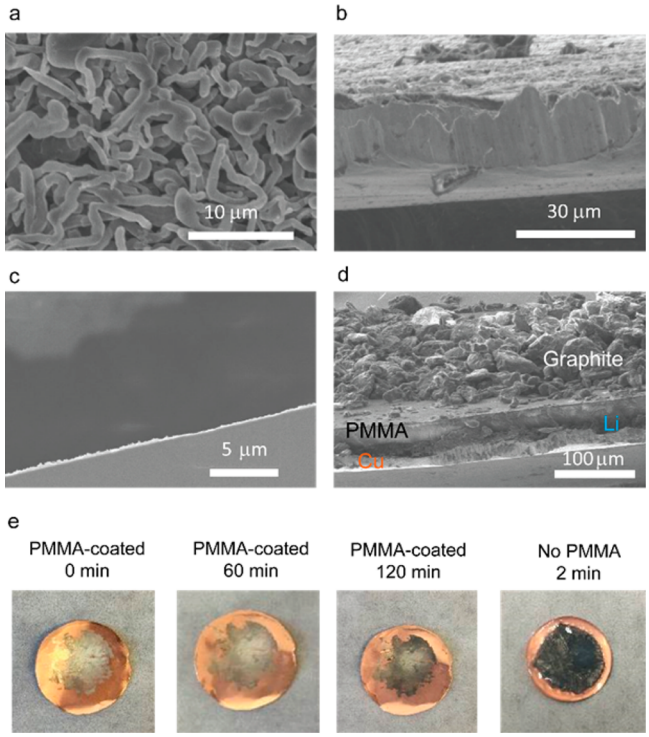

Figure 2. SEM characterizations and camera images of graphite/PMMA/lithium electrode. (a) Top view (a) and (b) side view (45°) of pure lithium film deposited onto copper. (c) Top view of PMMA-coated lithium. (d) Side view (45°) of graphite/PMMA/Li on copper. (e) Camera images of PMMA-coated lithium exposed to air with relative humidity of 30% for various time and lithium without PMMA coating.

indicates that the thickness is about 20 μm for 2 mAh Li/cm^2. Then 20 μL of 10 wt % PMMA in DOL was drop cast onto the lithium electrode inside a glovebox. After the DOL was evaporated, a uniform PMMA coating layer with a thickness of 20 μm was obtained (Figure 2c). The coating fully covers the lithium so that the lithium layer is not visible in this top view SEM image. The white line in Figure 2c is the edge of the electrode. Cracks were occasionally found, which could be removed with an optimized coating procedure. Then the sample was removed from the glovebox, and artificial graphite/PAA (90:10 in weight) in ethanol was drop cast onto PMMA-coated lithium, which results in a trilayer structure of graphite on PMMA and lithium (Figure 2d). To test the stability of the sample in ambient air, the PMMA-coated lithium film was exposed to air with relative humidity (RH) of 30% for various times. As seen in Figure 2e, the color of lithium remained largely white after 1 h, but turned dark after 2 h, suggesting that it was stable in air for ∼1 h. In contrast, a lithium film that is not protected by PMMA became dark after only 2 min in ambient air. This demonstrates that PMMA inhibits the

DOI: 10.1021/acs.nanolett.6b03655
Nano Lett. 2016, 16, 7235−7240

reaction of O_2 and H_2O with lithium and acts as a robust protecting layer to allow the slurry coating of anode and the fabrication steps in battery production.

To validate that lithium reacts with graphite when PMMA is dissolved, the graphite/PMMA/Li trilayer structure was soaked in a battery electrolyte (1 M $LiPF_6$ in EC/DEC) inside a coin cell. The amount of electrodeposited lithium was 1 mAh, whereas the mass of graphite was 1 mg. After aging for 24 h, the cell was opened and the graphite electrode appeared golden instead of black, which is the characteristic color of LiC_6 (Figure 3b).[29] To further prove the formation of lithiated

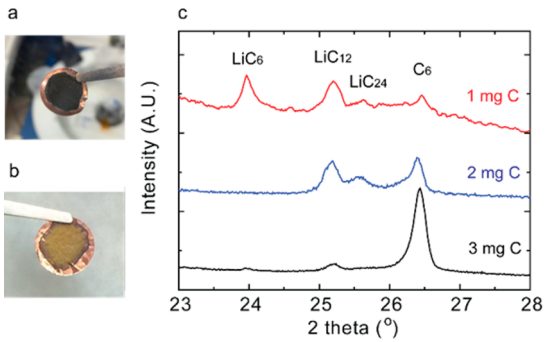

Figure 3. Camera images and XRD patterns of lithiated graphite. (a), (b) Graphite/PMMA/Li trilayer electrode before (a) and after (b) being soaked in battery electrolyte for 24 h. (c) XRD patterns of lithiated artificial graphite with various loadings. The lithiated graphite is made by sealing graphite/PMMA/lithium electrode with battery electrolyte (1 M $LiPF_6$ in EC/DEC) in a coin cell for 24 h.

graphite, X-ray diffraction patterns of graphite/PMMA/Li with various graphite loadings were taken. When the ratio of graphite to lithium is 3 mg/1 mAh, a graphite peak was still strong as the deposited lithium was not enough to fully lithiate graphite (black curve in Figure 3c). However, when the ratio was lowered to 1 mg/1 mAh (red curve in Figure 3c), graphite peaks almost disappeared, and only LiC_6 and LiC_{12} existed in the electrode, indicating that lithium was incorporated into graphite to form lithiated graphite electrode.[30]

XRD analysis and the color changes shown above indicate that lithium intercalates into the graphite structure in the graphite/PMMA/Li trilayer electrode. Followed by this success, the performance of the trilayer structure in ambient air was evaluated by electrochemical tests. In the test, electrochemically deposited lithium with a nominal capacity of 2 mAh/cm^2 was covered with PMMA followed by 3–4 mg/cm^2 artificial graphite. The graphite/PMMA/Li electrode was first exposed to air with fixed humidity for a certain period. Then the electrode was delithiated in a half cell with a Li metal counter electrode, so the amount of remaining active lithium in the lithiated graphite electrode can be determined. As shown in Figure 4a, when the electrode was not exposed to air, 1.18 mAh/cm^2 of lithium was extracted from the lithiated graphite. After exposing to 30% RH air for 30 and 60 min, the amount of Li extracted were 1.00 and 0.86 mAh/cm^2, respectively, which are 85% and 73% of that without exposure. Similarly, 0.98 and 0.78 mAh/cm^2 of Li remained active under exposing to 10% RH air for 1 and 6 h, respectively, which corresponded to 83% and 66% of that without exposure. These observations suggest that the unoptimized PMMA coating is already effective in protecting lithium for a period of ~60 min or longer in ambient air, which allows time for large-scale manufacturing. It should

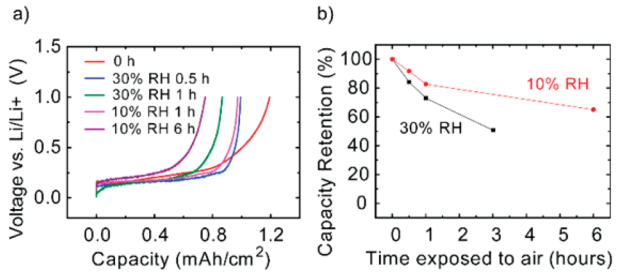

Figure 4. Effect of exposure to ambient air on the amount of active lithium in graphite/PMMA/Li electrode. (a) Delithiation from the graphite/PMMA/Li electrode in a half cell with lithium metal as the counter electrode. Different curves correspond to exposure to air for various times. The curves match the voltage profile of the graphite electrode. (b) Amount of active lithium extracted in the first delithiation versus time exposed to air. The capacity retention is normalized to the delithiated capacity without exposure.

be noted that the depth of lithiation corresponds to 250–300 mAh/g graphite in these cells, which means that the trilayer electrode structure not only compensates for lithium loss in the SEI but also provides a significant amount of active lithium that is available for lithium-free cathodes.

The experiment above also shows that lithium loss is as high as 40% even if the electrode is not exposed to air, as only 1.18 mAh/cm^2 is extracted with 2 mAh lithium/cm^2 deposited. This loss is attributed to the following reasons: (1) SEI formation in depositing lithium, which accounts for about 15% of capacity loss (Figure S1); (2) PMMA coating, as 1,3-dioxolane could further react with Li; and (3) SEI formation on graphite during the reaction between lithium and graphite in cell, which accounts for 5–10% of capacity loss based on the initial Coulombic efficiency of a standard graphite electrode prepared by the same method (Figure S2). Although lithium loss appears high, careful calculation suggests that it only affects energy density of a full cell up to 2%, because Li has an ultrahigh specific capacity of 3860 mAh/g, and thus the amount of Li consumed is very small. Detailed analysis can be found in the Supporting Information.

After initial delithiation, the graphite/PMMA/Li lithiated graphite electrode was further cycled at C/10 (1C = 372 mA/g), which was chosen because the Coulombic efficiency is typically low at a low current rate. Figure 5a shows the charge/discharge voltage curve in the first cycle after the initial delithiation (Figure 4). In this paper, the delithiation of the anode is associated with discharge, so the description is consistent with the full cell. Compared to a bare artificial graphite (AG) with an initial Coulombic efficiency of 92% (Figure S2), the graphite/PMMA/Li samples show high initial Coulombic efficiency of 99.7% and 99.0%, for exposure to 30% RH air for 30 min and 10% RH air for 60 min, respectively. These results clearly indicate that a high-quality SEI layer is formed during the initial lithiation process, so there is no further loss of lithium to form the SEI on graphite. The charge/discharge capacity is also comparable to bare AG. For samples exposed to 30% RH air for 30 min and 0% RH air for 60 min, the discharge specific capacity reached 318 and 328 mAh/g, respectively, which were close to 331 mAh/g of bare AG.

The exposure to ambient air also does not affect the cycling performance (Figure 5b). The specific capacity is stable for 30 cycles without noticeable decay, which is similar to bare AG. For example, after 30 min under 30% RH and 60 min under 10% RH, the discharge capacities reached 340 and 330 mAh/g

DOI: 10.1021/acs.nanolett.6b03655
Nano Lett. 2016, 16, 7235–7240

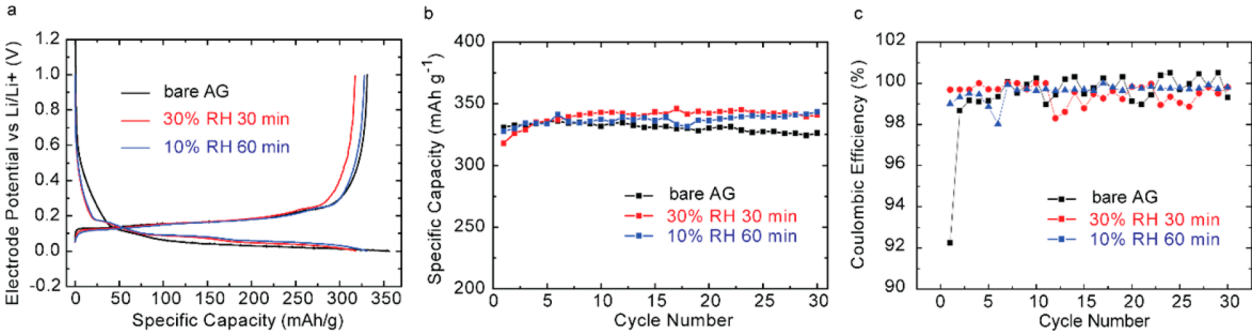

Figure 5. Electrochemical performance of the graphite/PMMA/Li structure. (a) Voltage profiles in the first charge/discharge cycle, which is comparable to the first charge/discharge cycle after the first delithiation in Figure 4a. (b) Cycling performance at C/10 (37.2 mA/g) for bare artificial graphite and after exposing to air for various time. (c) Coulombic efficiency of graphite/PMMA/lithium structure and bare AG. The initial Coulombic efficiencies reach 99.7% and 99.0% for exposing to 30% RH air for 30 min and 10% RH air for 60 min.

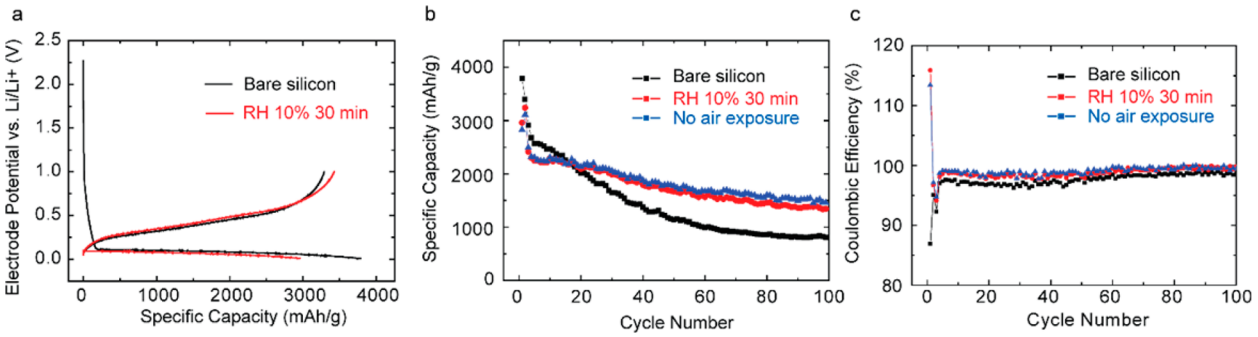

Figure 6. Electrochemical performance of Si nanoparticles/PMMA/lithium electrode. (a) Voltage profile of the first charge/discharge cycle of Si NP/PMMA/Li electrode and a bare Si electrode at C/20. The Si NP/PMMA/Li electrode has less charge capacity than discharge capacity as lithium is incorporated into silicon during the lithiation process. (b), (c) Cycling performance (b) and Coulombic efficiency (c) of bare Si NP electrodes, Si NP/PMMA/Li electrode exposed to 10% RH air for 30 min, and Si NP/PMMA/Li electrode not exposed to air. The cycling is performed at C/2, except that the first two cycles are at C/20.

after 30 cycles, respectively. The increasing capacity is likely a result of better electrolyte wetting and redistribution of PMMA in the electrolyte. Meanwhile, the specific discharge capacity is 327 mAh/g after 30 cycles for bare AG. The average Coulombic efficiency over 30 cycles are as high as 99.62 and 99.71% for 30 min under 30% RH and 60 min under 10% RH, respectively, which are comparable to 99.77% for bare AG. These results show that the cycling performance of AG/PMMA/lithium electrodes are as stable as bare AG.

After validating the electrochemical performance of the lithiated graphite anode, the proposed strategy was further validated with silicon nanoparticles (NPs). The silicon nanostructures exhibit significant capacity loss due to volume expansion of Si, and the large surface area leads to significant SEI formation. Thus, the initial Coulombic efficiency is typically as low as 70−80%.[9,10,14] Therefore, prelithiation is attractive to compensate for the lithium loss in the SEI. To test our strategy, Si nanoparticles (<80 nm, US Research Nanomaterials Inc.) were dispersed in ethanol together with 15 wt % of carbon black and 15 wt % PAA binder to form a slurry that was coated on the PMMA-protected Li electrode outside a glovebox. In this electrode, the mass loading was 0.4−0.6 mg Si/cm^2 and the predeposited lithium on copper was 1.0 mAh/cm^2. The electrode was pressed at 2 MPa for 1 min so that the Si nanoparticles in the electrode formed a better connected network, but the direct contact between Si nanoaprticles and lithium was avoided. SEM images show that after PMMA dissolution and lithiation of Si nanoparticles, the particle size grows from ∼50 nm to ∼100 nm, which is evidence for prelithiation and SEI formation (Figure S3).

The electrochemical performance of the Si/PMMA/Li and bare Si NPs electrodes are shown in Figure 6. The bare Si NP electrode has an initial Coulombic efficiency of only 87% at C/20 (1C = 4000 mA/g), indicating that 13% of lithium is consumed by the SEI layer. In contrast, the discharge capacity of the Si NP/PMMA/lithium electrode (3426 mAh/g) is higher than the charge capacity (2961 mAh/g) because prelithiation "charges" Si NP prior to electrochemical lithiation (Figure 6a). Therefore, there should not be any capacity loss in the initial charging due to SEI formation. After two cycles at C/20, Si electrodes were further charged/discharged at C/2. While the bare silicon sample only has a capacity of 809 mAh/g after 100 cycles, the Si/PMMA/lithium sample exposed to air with 10% RH air for 30 min has a capacity of 1340 mAh/g after 100 cycles, corresponding to 58% retention. This capacity also approaches the result of Si/PMMA/lithium electrode not exposed to air, which is 1456 mAh/g after 100 cycles, or 63% capacity retention, suggesting that the exposure to air does not significantly affect the cycling performance. The improved capacity retention compared to bare Si NPs is possibly a result of strain relaxation in the initial lithiation process. Along with improved cycling performance, the average Coulombic efficiency from cycle 5 to 100 also improves from 98.1% for the bare Si sample to 98.9% for the Si/PMMA/lithium electrode exposed to 10% RH air for 30 min. These results suggest that the proposed prelithiation strategy is effective for Si electrodes. However, we would like to point out that the

DOI: 10.1021/acs.nanolett.6b03655
Nano Lett. 2016, 16, 7235−7240

stability of the Si electrode in ambient air is not as good as graphite. When the humidity reaches 30%, or exposure time is over 1 h in air with 10% RH, the improvement in electrochemical performance vanishes quickly. This may be related to the fact that silicon is more hydrophilic and has a much larger surface area than graphite, so that moisture penetrates the active material−PMMA layer more easily.

To verify this strategy that the ambient-air-stable lithiated anode forms a stable SEI but also permits a fully lithiated anode to be paired with a Li-free cathode, a full cell with graphite/PMMA/Li anode and $Li_4Ti_5O_{12}$ cathode was assembled and tested. The test acts as the first step toward Li-ion batteries with high-capacity lithiated anode and lithium-free cathode (e.g., sulfur/Li_xSi system).[13] There are two reasons to choose $Li_4Ti_5O_{12}$: (1) It does not contain active lithium, so the only lithium source in the system is lithiated graphite. (2) It has excellent cycling performance and nearly 100% Coulombic efficiency, and thus any degradation observed in full cell cycling is mainly due to the lithiated graphite electrode. By isolating degradation to the lithiated graphite, we have a better understanding of the origin of performance deterioration and helps to further improve the lithiated anode. The lithiated graphite electrode was exposed to air with 30% RH for 30 min before assembly. In the full cell test, the total available amount of lithium is targeted to be 20% higher than the theoretical capacity of LTO (175 mAh/g). As shown in Figure 7a, the

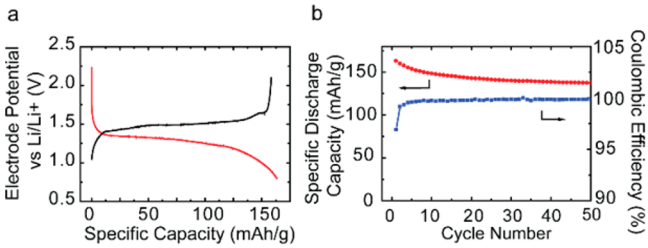

Figure 7. Electrochemical performance of $Li_4Ti_5O_{12}$/ graphite/PMMA/Li full cell. (a) Voltage profile at a current rate of C/10 based on capacity of graphite. (b) Corresponding cycle life and Coulombic efficiency.

average charging and discharging voltages are 1.5 and 1.3 V, respectively, which is consistent with the electrode potential of LTO (1.55 V vs Li/Li^+) and graphite (0.1−0.2 V vs Li/Li^+). The initial discharge capacity was as high as 163 mAh/g, which also corresponds to 302 mAh/g for the graphite anode. The capacity is 137 mAh/g after 50 cycles, corresponding to a retention of 84%. Moreover, the capacity decay rate is only 0.089% per cycle at the end of 50 cycles. The loss is likely a result of lithium consumption during the reaction, such as trace amount of water in LTO and the <100% Coulombic efficiency of the graphite electrode. This full cell performance supports the proposal that the air-stable lithiated electrode can be paired with high-capacity lithium-free cathode material for a full cell.

The studies above clearly show that the proposed electrode structure acts as a lithiated anode to compensate SEI loss and readily paired with a lithium-free cathode. One key step in the design is that the solvent to disperse anode materials should not dissolve the polymer coating, and ethanol was used in this report. Although ethanol was studied as a solvent for battery coatings and is environmentally friendly, water is preferred because it is the greenest solvent. In principle, water is used because it does not dissolve PMMA and has a low permeability in PMMA.[31] A preliminary test shows that a PMMA-coated lithium electrode is also stable for a certain period when it is in contact with water. For example, when 2 mAh/cm^2 lithium was coated with 20 μm PMMA, the lithium color remained unchanged for 5 min, and gradually becomes dark after 10 min (Figure S4a). Another sample, which is 750 μm of commercial lithium foil coated with 100 μm of PMMA, is stable for over 30 min in contact with water (Figure S4b). Therefore, this strategy has the potential to be compatible with an aqueous slurry, which is widely used in anode coating.

Another potential concern of this strategy to prepare ambient-air-stable lithiated anode is the contact between lithiated particles and the metal substrate. We have not observed issues due to electrical contact between lithiated particles and metal substrates in coin cell and pouch cell tests. This is possibly a result of both expansion of particles after lithiation and pressure inside cells. However, further tests are needed to examine the validity of this approach in scaling up to cylindrical and prismatic cells.

In summary, we describe a new electrode structure that is developed to fabricate lithiated battery anodes. In these electrodes, metallic lithium is first protected by a PMMA layer against air and moisture. Then active materials, such as artificial graphite or silicon nanoparticles, are coated onto PMMA in a solvent (e.g., ethanol) that does not dissolve PMMA. Because PMMA is readily soluble in battery electrolytes, anode materials are in situ lithiated in a cell to form a lithiated anode. In principle, such a process could transfer to other battery systems such as Na-ion and K-ion batteries. The electrode shows stability in ambient air under normal humidity (10−30%) for reasonable amount of time (30−60 min). The process also has the potential to be integrated with standard battery fabrication processes, especially after further optimization and improvement.

Chemicals. Artificial graphite is purchased from MTI Corp., and lithium bis(trifluoromethane)sulfonimide (LiTFSI), 1,3-dioxolane, poly(methyl methacrylate), and poly(acrylic acid) are purchased from Sigma-Aldrich. The lithium metal foil is purchased from Alfa Aesar. Timical Super C45 carbon back is used as-received. The poly(vinylidene fluoride) (PVdF) is obtained from Kynar. Si nanoparticles with diameter <80 nm is purchased from US Research Nanomaterials Inc. $Li_4Ti_5O_{12}$, was obtained from HydroQuebec.

Electrode Preparation. The graphite/PMMA/lithium trilayer structure was prepared by the following steps. Lithium was first electrochemically deposited at 1 mA/cm^2 on copper in 1 M LiTFSI/1,3-dioxolane in a half cell. Then the half cell was opened in a glovebox and the lithium on copper electrode was washed with 1,3-dioxolane and dried. Then, 20 μL 10 wt % PMMA ($M_w \sim 120\,000$) in 1,3-dioxolane was drop cast onto the lithium electrode inside a glovebox with O_2 < 0.1 ppm and H_2O < 0.1 ppm. A uniform PMMA coating layer with a thickness of 20 μm was obtained after the dioxolane evaporated. Then the sample was removed from the glovebox, and graphite/PAA (90:10 in weight) in ethanol was drop cast onto the PMMA-coated lithium electrode. The weight ratio of solid to liquid was 1:9 in the slurry. For the silicon NP electrodes, Si NPs were mixed with PAA and carbon black in ethanol with a weight ratio of 70:15:15. The typical mass loading was 3−5 mg/cm^2 for graphite and 0.4−0.6 mg/cm^2 for Si.

Material Characterizations. X-ray diffraction was performed with a PANalytical XPert3 Powder XRD. SEM images

DOI: 10.1021/acs.nanolett.6b03655
Nano Lett. 2016, 16, 7235−7240

were obtained by a Hitachi S-4700 SEM. An environment with a constant humidity was created by flowing dry air continuously in a sealed vacuum chamber for various times. Then the gas flow was stopped, and the humidity remains constant. The relative humidity was monitored by an easy-to-read humidity meter (McMaster Carr).

Battery Assembly. The anode/PMMA/Li electrode was assembled together with a lithium metal counter electrode in a pouch cell. The electrolyte was 1 M $LiPF_6$ in EC/DEC (Selecliyte LP40). For the full cell, $Li_4Ti_5O_{12}$ was used as the positive electrode, which was made by mixing with 10% PVdF and 10% carbon black in NMP (*N*-methyl-2-pyrrolidone) that was coated onto an Al substrate.

Electrochemical Measurement. Galvanostatic cycling was performed in a pouch cell using either a Biologic VMP3 battery tester or a Landt Battery tester. The electrolyte is 1 M $LiPF_6$ in 1:1 ethylene carbonate and diethyl carbonate (BASF). The separator is polypropylene−polyethylene−polypropylene tri-layer separator purchased from MTI.

■ ASSOCIATED CONTENT

Supporting Information

The Supporting Information is available free of charge on the ACS Publications website at DOI: 10.1021/acs.nanolett.6b03655.

Initial cycle of lithium deposition and stripping, initial cycle of artificial graphite electrode, effect of lithium loss on battery energy density, prelithiated Si electrode, exposure of PMMA-protected lithium to water droplet. (PDF)

■ AUTHOR INFORMATION

Corresponding Author

*E-mail: yy2664@columbia.edu.

Notes

The authors declare no competing financial interest.

■ ACKNOWLEDGMENTS

Y.Y. acknowledges support for startup funds from Columbia University and seed fund from Lenfest Center for Sustainable Energy at Columbia University.

■ REFERENCES

(1) Chu, S.; Majumdar, A. *Nature* **2012**, *488* (7411), 294−303.
(2) Whittingham, M. S. *MRS Bull.* **2008**, *33* (4), 411−419.
(3) Choi, N. S.; Chen, Z. H.; Freunberger, S. A.; Ji, X. L.; Sun, Y. K.; Amine, K.; Yushin, G.; Nazar, L. F.; Cho, J.; Bruce, P. G. *Angew. Chem., Int. Ed.* **2012**, *51* (40), 9994−10024.
(4) Tarascon, J. M.; Armand, M. *Nature* **2001**, *414* (6861), 359−367.
(5) Palacin, M. R.; de Guibert, A. *Science* **2016**, *351* (6273), 1253292.
(6) Yoshio, M.; Wang, H. Y.; Fukuda, K.; Hara, Y.; Adachi, Y. *J. Electrochem. Soc.* **2000**, *147* (4), 1245−1250.
(7) Ohzuku, T.; Iwakoshi, Y.; Sawai, K. *J. Electrochem. Soc.* **1993**, *140* (9), 2490−2498.
(8) Zhao, H.; Yuan, W.; Liu, G. *Nano Today* **2015**, *10* (2), 193−212.
(9) McDowell, M. T.; Lee, S. W.; Nix, W. D.; Cui, Y. *Adv. Mater.* **2013**, *25* (36), 4966−4984.
(10) Chan, C. K.; Peng, H.; Liu, G.; McIlwrath, K.; Zhang, X. F.; Huggins, R. A.; Cui, Y. *Nat. Nanotechnol.* **2008**, *3* (1), 31−35.
(11) Liu, N.; Lu, Z.; Zhao, J.; McDowell, M. T.; Lee, H.-W.; Zhao, W.; Cui, Y. *Nat. Nanotechnol.* **2014**, *9* (3), 187−192.
(12) Son, I. H.; Park, J. H.; Kwon, S.; Park, S.; Rummeli, M. H.; Bachmatiuk, A.; Song, H. J.; Ku, J.; Choi, J. W.; Choi, J. M.; Doo, S. G.; Chang, H. *Nat. Commun.* **2015**, *6*, 7393.
(13) Liu, N. A.; Hu, L. B.; McDowell, M. T.; Jackson, A.; Cui, Y. *ACS Nano* **2011**, *5* (8), 6487−6493.
(14) Kim, H. J.; Choi, S.; Lee, S. J.; Seo, M. W.; Lee, J. G.; Deniz, E.; Lee, Y. J.; Kim, E. K.; Choi, J. W. *Nano Lett.* **2016**, *16* (1), 282−288.
(15) Yang, Y.; McDowell, M. T.; Jackson, A.; Cha, J. J.; Hong, S. S.; Cui, Y. *Nano Lett.* **2010**, *10* (4), 1486−1491.
(16) Zhao, J.; Lu, Z. D.; Wang, H. T.; Liu, W.; Lee, H. W.; Yan, K.; Zhuo, D.; Lin, D. C.; Liu, N.; Cui, Y. *J. Am. Chem. Soc.* **2015**, *137* (26), 8372−8375.
(17) Sun, Y. M.; Lee, H. W.; Zheng, G. Y.; Seh, Z. W.; Sun, J.; Li, Y. B.; Cui, Y. *Nano Lett.* **2016**, *16* (2), 1497−1501.
(18) Park, K.; Yu, B.-C.; Goodenough, J. B. *Adv. Energy Mater.* **2016**, *6* (10), 1502534.
(19) Forney, M. W.; Ganter, M. J.; Staub, J. W.; Ridgley, R. D.; Landi, B. J. *Nano Lett.* **2013**, *13* (9), 4158−4163.
(20) Zhao, H.; Wang, Z.; Lu, P.; Jiang, M.; Shi, F.; Song, X.; Zheng, Z.; Zhou, X.; Fu, Y.; Abdelbast, G.; Xiao, X.; Liu, Z.; Battaglia, V. S.; Zaghib, K.; Liu, G. *Nano Lett.* **2014**, *14* (11), 6704−6710.
(21) Wang, L.; Fu, Y.; Battaglia, V. S.; Liu, G. *RSC Adv.* **2013**, *3* (35), 15022−15027.
(22) Bruce, P. G.; Freunberger, S. A.; Hardwick, L. J.; Tarascon, J.-M. *Nat. Mater.* **2011**, *11* (1), 19−29.
(23) Bridel, J. S.; Azais, T.; Morcrette, M.; Tarascon, J. M.; Larcher, D. *Chem. Mater.* **2010**, *22* (3), 1229−1241.
(24) Li, J.; Lewis, R. B.; Dahn, J. R. *Electrochem. Solid-State Lett.* **2007**, *10* (2), A17−A20.
(25) Magasinski, A.; Zdyrko, B.; Kovalenko, I.; Hertzberg, B.; Burtovyy, R.; Huebner, C. F.; Fuller, T. F.; Luzinov, I.; Yushin, G. *ACS Appl. Mater. Interfaces* **2010**, *2* (11), 3004−3010.
(26) Kim, H. T.; Kim, K. B.; Kim, S. W.; Park, J. K. *Electrochim. Acta* **2000**, *45* (24), 4001−4007.
(27) Hjelm, A. K.; Eriksson, T.; Lindbergh, G. *Electrochim. Acta* **2002**, *48* (2), 171−179.
(28) Deka, M.; Kumar, A. *Electrochim. Acta* **2010**, *55* (5), 1836−1842.
(29) Lee, C. M.; Yang, S. H.; Mun, B. J.; Ross, P. N. *Surf. Sci.* **2001**, *477* (2−3), 126−132.
(30) Jiang, J.; Dahn, J. R. *Electrochem. Solid-State Lett.* **2003**, *6* (9), A180−A182.
(31) Lee, W. J.; Ju, S. P. *J. Phys. Chem. B* **2009**, *113* (40), 13269−13278.

DOI: 10.1021/acs.nanolett.6b03655
Nano Lett. 2016, 16, 7235−7240